Phase-Separation and Domain-Formation in Cholesterol-Sphingomyelin Mixture: Pulse-EPR Oxygen Probing

Laxman Mainali,[†] Marija Raguz,[†‡] and Witold K. Subczynski[†*]
[†]Department of Biophysics, Medical College of Wisconsin, Milwaukee, Wisconsin; and [‡]Department of Medical Physics and Biophysics, School of Medicine, University of Split, Split, Croatia

ABSTRACT Membranes made of Chol/ESM (cholesterol/egg sphingomyelin) mixtures were investigated using saturation-recovery electron paramagnetic resonance spin-labeling methods, in which bimolecular collisions of relaxation agents (oxygen or nickel ethylenediamine diacetic acid) with spin labels are measured. Liquid-disordered (l_d) and liquid-ordered (l_o) phases, and cholesterol bilayer domains (CBDs) were discriminated and characterized by profiles of the oxygen transport parameter (OTP). In the l_d phase, coexisting with the l_o phase, the OTP profile is bell-shaped and lies above that in the pure ESM membrane. Changes in the OTP profile across the l_o phase are complex. When the l_o phase coexists with the l_d phase, the OTP profile is similar to that across the pure ESM membrane but with a steeper bell shape. With an increase in cholesterol concentration (up to the cholesterol-solubility threshold), the profile becomes rectangular, with low OTP values from the membrane surface to the depth of C9, and high values in the membrane center. This approximately threefold increase in the OTP occurs at the depth at which the rigid ring structure of cholesterol is immersed. Further addition of cholesterol and the formation of the CBD does not affect the OTP profile across the l_o phase. OTP values in the CBD are significantly lower than in the l_o phase.

INTRODUCTION

Our motivation for undertaking studies on membranes made from cholesterol/egg sphingomyelin (Chol/ESM) mixtures is twofold. First, we are interested in the role of cholesterol in forming membrane domains, especially raft domains (1–5). Second, we are interested in the properties and organization of lipids in fiber cell plasma membranes of the eye lens (6–10). In our investigations, we extensively used electron paramagnetic resonance (EPR) spin-labeling methods to study the organization and dynamics of phospholipid membranes with different cholesterol contents. Here, cholesterol not only saturates the phospholipid bilayer but also leads to the formation of immiscible cholesterol bilayer domains (CBDs) (3,5,7–9,11,12). These methods provide a unique opportunity to determine the lateral organization of membranes, including the investigation of coexisting membrane phases and domains. Furthermore, these methods present additional opportunities to determine several important membrane properties as a function of bilayer depth, including alkyl chain order (13), membrane fluidity (12), hydrophobicity (14), and the oxygen diffusion-concentration product (called the oxygen transport parameter (OTP)) (15,16). In some cases, these properties can be obtained in coexisting membrane phases and domains (3,4,8,9,11,12,17).

Rafts are considered to be representative of dynamic domains in the cell membrane requiring both cholesterol and sphingolipids. The operational definition of lipid rafts (which is closely related to our research) states that "depletion of either cholesterol or sphingolipids from cell membranes leads to the disappearance of the detergent-resistant fraction and the loss (or modulation) of specific membrane functions (signaling events) connected with rafts" (18). EPR spin-labeling provides information on the organization and dynamics of raft molecules, as well as the organization and dynamics of the raft itself in the membrane (1–3). Our results support the definition of rafts formulated by Pike (19), which states that: "Membrane rafts are small (10–200 nm), heterogeneous, highly dynamic, sterol- and sphingolipid-enriched domains that compartmentalize cellular processes. Small rafts can sometimes be stabilized to form larger platforms through protein-protein and protein-lipid interactions." It is believed that raft domains are in the liquid-ordered (l_o) phase (20–22). Thus, raft researchers can gain some insight into the structure of and molecular interactions in raft domains by understanding l_o phases and liquid-liquid phase separations in binary or ternary mixtures of lipids, including cholesterol and saturated-chain lipids. Ternary lipid mixtures containing cholesterol, saturated, and unsaturated phospholipids (PLs) were investigated to confirm the existence of the l_o phase and to describe regions of phase diagrams where this phase coexists with the liquid-disordered (l_d) phase (23–26). These results clearly show that in the investigated systems the l_o phase domain is formed and coexists with the l_d phase domain when the saturated PL is sphingomyelin (23,24) or distearoylphosphatidylcholine (25). These domains are much smaller than the optical resolution limit and cannot be discriminated by fluorescence microscopy (27). Estimated sizes vary from ~2–8 nm (25) to 45–70 nm (24). These works also discuss whether cholesterol/PL (Chol/PL) interactions are better described as l_o and

Submitted March 3, 2011, and accepted for publication July 13, 2011.

*Correspondence: subczyn@mcw.edu

Editor: David D. Thomas.

0006-3495/11/08/0837/10 $2.00

doi: 10.1016/j.bpj.2011.07.014

l_d coexisting phases or as condensed complexes of PL and cholesterol (28).

Using the unique abilities of EPR spin-labeling methods, we found (3) that the commonly accepted statement that properties of the l_o phase lie between those for the l_d and solid-ordered (s_o) phases (29) is true for membranes formed at a low Chol/PL mixing ratio where the l_o phase coexists with the l_d or s_o phase. However, at higher cholesterol contents, the OTP in the l_o phase is similar to that in the s_o phase from the membrane surface to the depth of C9 and to that in the l_d phase at depths deeper than C9, showing that the cholesterol-based l_o phase is ordered only near the membrane surface and still retains a high level of disorder in the bilayer center. This property may facilitate lateral mobility in l_o phases. Thus, investigation of the molecular dynamics and structures in the direction of the depth in the coexisting or separated phases and domains is especially important.

Our earlier research was carried out to characterize the physical properties of the l_o phase when it coexists with either the l_d or s_o phase. We employed one of the most straightforward model membranes containing the l_o phase: a binary mixture of dimyristoylphosphatidylcholine (DMPC) and cholesterol (3). We also made preliminary measurements on Chol/ESM binary mixtures. The effects of cholesterol on membrane order and the OTP were monitored at the depth of C5 in fluid- and gel-phase ESM membranes (4).

Recently, our attention became focused on the unique composition of the fiber cell plasma membranes of the eye lens, which have the highest cholesterol content of any known biological membrane. In human lenses, the Chol/PL molar ratio varies from 1:1 to 2:1 in the cortex to as high as 3:1–4:1 in the nucleus (30). The PL composition of the fiber cell plasma membrane changes drastically with age, with the preferential depletion of glycerol-PLs and the consequent enrichment of sphingolipids (31). Sphingolipids (mainly, sphingomyelin (SM) and dihydro-SM) account for 66% or more of the total PLs in the eye lens of the adult human (32). The high, saturating level of cholesterol, affects the organization of lipids in fiber cell plasma membranes, including the formation of the l_o phase and immiscible, pure CBDs. The effects of cholesterol should be strongly modulated by the presence of sphingolipids. The alkyl chains of these PLs are highly saturated. Additionally, cholesterol solubility in sphingolipid bilayers is extremely high. The cholesterol solubility threshold (CST) reported for these membranes is at a Chol/SM molar ratio of 2:1 (33), compared with CSTs in phosphatidylcholine (PC), phosphatidylethanolamine, and phosphatidylserine membranes at Chol/PL molar ratios of 1:1 (34), 1:1 (35), and 1:2 (36), respectively.

In our present research, we discriminated phases and domains in membranes made of Chol/ESM mixing ratios from 0 to 3. Both cholesterol (cholestane spin label (CSL) and androstane spin label (ASL)) and PL analog spin labels (*n*-PC and *n*-SASL) were used (see Fig. S1 in the Supporting Material). These spin labels have molecular structures similar to parent cholesterol or PLs and, therefore, are expected to behave and similarly distribute across different membrane domains. Experiments carried out with probe molecules necessitate due caution in interpreting results; the labeled molecules cannot be expected to mimic all of the properties of cholesterol or PLs. Nevertheless, the interaction of CSL (or ASL) with PL and/or cholesterol should, to a certain degree, approximate cholesterol-PL and cholesterol-cholesterol interactions in the membrane domain because of the overall similarity in their molecular structures and phase behaviors in PC-cholesterol membranes (37). Similarly, phase boundaries drawn for Chol/DMPC membranes contain points obtained with *n*-PCs (38). Furthermore, points obtained with *n*-SASLs (5) fit perfectly to these boundaries. Phase boundaries obtained with 5-SASL for Chol/ESM (4) overlap appropriate boundaries in the phase diagram for Chol/palmitoyl-SM (PSM) presented by Almeida et al. (39).

We also characterized three-dimensional dynamic structures of these phases and domains at cholesterol contents where they coexisted or occupied the entire membrane. This was possible through the use of a very small probe (i.e., molecular oxygen). With this approach, a variety of phospholipid spin labels were incorporated into the membrane to probe specific depths and domains (see Fig. S1). The rate of collision between molecular oxygen and the nitroxide moiety attached to a specific location in the lipid was measured using the saturation-recovery (SR) EPR method. The oxygen collision rate (a product of the local concentration and the local diffusion coefficients of molecular oxygen within the membrane) is a very sensitive monitor of membrane fluidity that reports on translational diffusion of molecular oxygen (15). Detailed profiles of oxygen collision rates, or the OTP, were obtained for Chol/ESM mixing ratios, shown as solid dots in the phase diagram of Fig. 1. The temperature at which experiments were performed (40°C) is indicated by a broken line. Fig. 1 also contains a schematic drawing of the organization of lipid molecules in phases and/or domains that should exist at certain cholesterol contents. Fig. 1 should be used as a guideline for the presentation and interpretation of our data.

MATERIALS AND METHODS

Materials

ESM, cholesterol, and phospholipid spin labels (1-palmitoyl-2-(*n*-doxylstearoyl)phosphatidylcholine (*n*-PC, where $n = 5, 7, 10, 12, 14$, or 16) or tempocholine-1-palmitoyl-2-oleoylphosphatidic acid ester (T-PC) were obtained from Avanti Polar Lipids (Alabaster, AL). Nine-doxylstearic acid spin labels (9-SASL), CSL, and ASL were purchased from Molecular

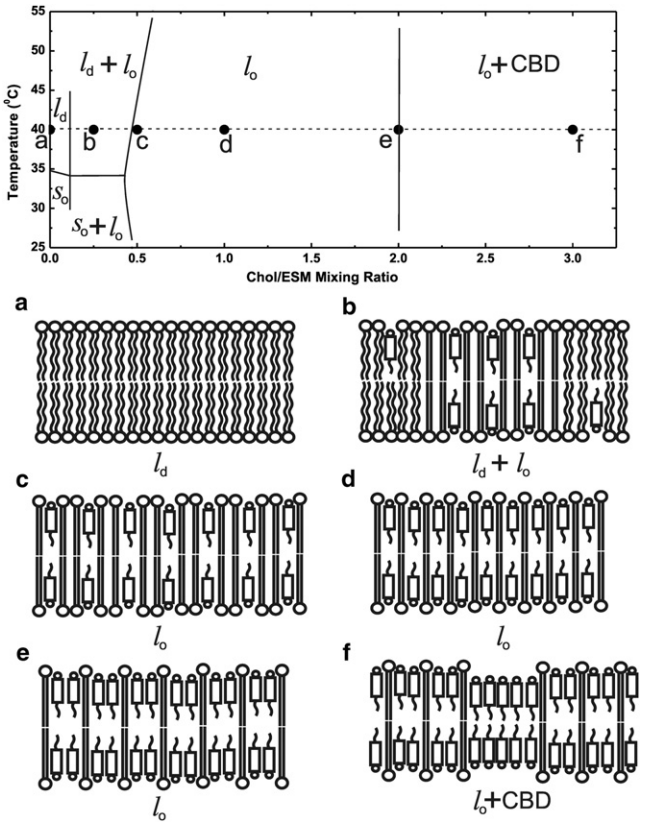

FIGURE 1 Phase diagram of the Chol/ESM membrane. The broken line and solid circles indicate the temperature and Chol/ESM mixing ratios at which measurements were performed. Schematic drawings of membrane structures (including phases and domains) at different Chol/ESM mixing ratios ((*a*) 0; (*b*) 1:4; (*c*) 1:2; (*d*) 1:1; (*e*) 2:1; (*f*) 3:1) are presented.

Probes (Eugene, OR). Other chemicals (of at least reagent grade) were purchased from Sigma-Aldrich (St. Louis, MO).

Preparation of Chol/ESM membranes

The membranes used in this study were multilamellar dispersions of ESM and cholesterol containing 1 mol % spin label. The membranes were prepared using the film deposition method as described in (5). Chloroform solutions of ESM, cholesterol, and spin label were mixed to attain a desired mixing ratio. Chloroform was evaporated with a stream of nitrogen and with the test tube in constant rotation so as to deposit a uniform film of lipid over the bottom of the tube. The lipid film was thoroughly dried under reduced pressure (0.1 mm Hg) for 12 h. A buffer solution (0.2 ml of 10 mM PIPES and 150 mM NaCl, pH 7.0) was added to the dried lipids at 50°C and vigorously mixed. The buffer used for samples with 9-SASL was 0.1 M borate at pH 9.5. A rather high pH was chosen in this case to ensure that all 9-SASL carboxyl groups were ionized in the ESM membranes (40). The properties of ESM membranes should not be sensitive to a pH range of ~5–~11 because ionization of ESM polar PC headgroups does not change in this pH range (41).

To avoid traces of solvent (chloroform) in our samples (and due to the uncertainty of chloroform removal efficiency (42)), we did not use the rapid solvent exchange method (35) in our preparations. Instead, we used the film deposition method, which is widely used (39,43,44). A significant advantage of the film deposition method in the application of EPR spin labeling to discriminate and characterize the CBD (which was demonstrated and described in detail in our previous work (9)) is that the EPR signal of ASL and CSL from cholesterol crystals is so broad that it cannot be seen in conditions where the signal from CBD is recorded.

EPR measurements

The membranes were centrifuged briefly, and the loose pellet was used for EPR measurements. The sample was placed in a 0.6 mm i.d. capillary made of a gas-permeable methylpentene polymer called TPX (45). Conventional EPR spectra were routinely recorded for all samples with a Bruker EMX spectrometer equipped with temperature control accessories. Samples were thoroughly deoxygenated, yielding correct EPR line-shapes. The z-component of the hyperfine interaction tensor, A_Z, for ASL and CSL in the membrane was determined directly from EPR spectra for samples frozen at about –165°C and recorded with a modulation amplitude of 2.0 G and an incident microwave power of 2.0 mW (14).

SR measurements were performed using an SR EPR X-band spectrometer equipped with a loop-gap resonator (46). Spin-lattice relaxation times (T_1s) were determined by analyzing the SR signal of the central line obtained in short pulse experiments (16,46). For measurements of the OTP, the sample was equilibrated with the same gas that was used for temperature control (i.e., a controlled mixture of nitrogen and dry air adjusted with flowmeters (Matheson Gas Products, Montgomery, PA, model 7631H-604)) (15,47). A relatively low level of observing power (8 μW, with the loop-gap resonator delivering an H_1 field of 3.6×10^{-5} G) was used for all experiments to avoid microwave power saturation (which induces artificial shortening of the apparent T_1). Typically, $10^5 - 10^6$ decays were acquired with 2048 data points on each decay. Sampling intervals 2, 2.5, 4, 5, 10, or 20 ns were used for measurements. The total accumulation time was typically 2–5 min.

SR signals were fitted by single- or double-exponential functions. When a single exponential fit was satisfactory, the decay time constant was evaluated with a standard deviation smaller than $\pm 3\%$ from the mean value for independent experiments (for samples prepared totally independently). When a double-exponential fit was necessary, and satisfactory, the decay times were usually evaluated with standard deviations $< \pm 5\%$ and $\pm 10\%$ for longer and shorter recovery time constants, respectively. Larger standard deviations for shorter components are due to the difficulty in measuring very short T_1s (due to the presence of molecular oxygen) in the current setting of the instrument. It is also possible that the available pump power cannot saturate the signal when the T_1 is very short.

The outline of theory for evaluating the OTP and nickel ethylenediamine diacetic acid (NiEDDA) accessibility parameter is given in the Supporting Material.

RESULTS AND DISCUSSION

Discrimination of membrane phases and domains using PL-analog spin labels

Fig. 1 is the guideline for our experiments. All measurements were performed in fluid-phase membranes. We chose 40°C to ensure that measurements were performed well above the phase transition temperature of ESM membranes (~35°C), which is somewhat broad because of the natural source of this PL (4,39,43,48). Six Chol/ESM mixing ratios (indicated in Fig. 1 as *black dots*) represent cholesterol contents at which phases and/or domains either exist as single structures or coexist.

Fig. 2 contains representative SR signals for 7-PC in ESM membranes with different cholesterol contents. We chose 7-PC because we expected it to present pronounced changes in T_1 in the presence of oxygen. In deoxygenated samples,

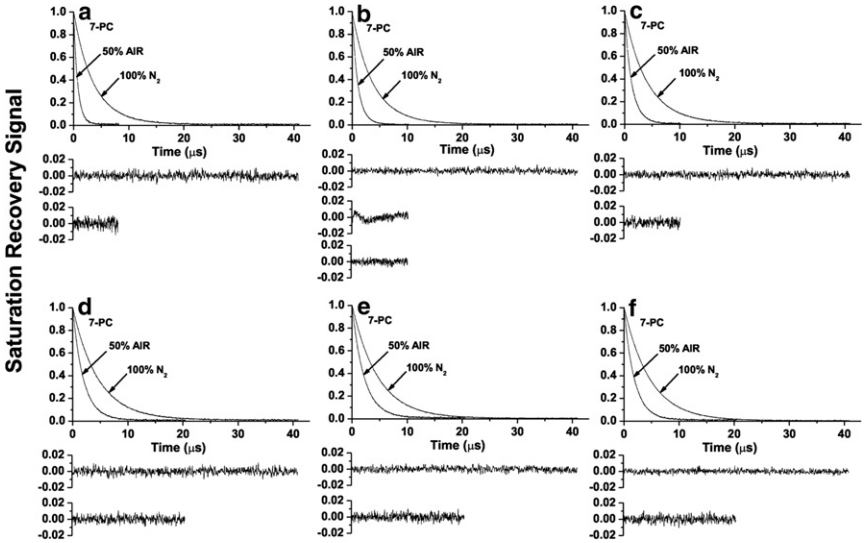

FIGURE 2 Representative SR signals with fitted curves and residuals (the experimental signal minus the fitted curve) of 7-PC obtained at different Chol/ESM mixing ratios (indicated in Fig. 1). Membrane specimens were equilibrated with nitrogen or a mixture of 50% air and 50% nitrogen. SR signals were satisfactorily fitted to a single-exponential function in the absence of molecular oxygen with time constants of (*a*) 3.56 ± 0.01 μs, (*b*) 3.78 ± 0.01 μs, (*c*) 4.12 ± 0.01 μs, (*d*) 4.59 ± 0.01 μs, (*e*) 4.62 ± 0.01 μs, and (*f*) 4.66 ± 0.01 μs. SR signals in the presence of molecular oxygen were fitted either to single exponentials with time constants of (*a*) 0.73 ± 0.01 μs, (*c*) 1.25 ± 0.01 μs, (*d*) 1.94 ± 0.01 μs, (*e*) 2.00 ± 0.01 μs, (*f*) 1.86 ± 0.01 μs, or double exponentials with time constants of (*b*) 1.19 ± 0.05 μs and 0.60 ± 0.06 μs (the middle residual in *b* is for single- and the lower residuals for double-exponential fits).

SR signals for 7-PC were fitted successfully to a single-exponential function, indicating that the spin label alone cannot discriminate purported domains. Similarly, single-exponential curves were good fits for other PL spin labels in deoxygenated samples. SR signals from samples equilibrated with 50% air were also single exponential. Only for samples at a Chol/ESM mixing ratio of 1:4 (Fig. 2 *b*) could the SR signal for 7-PC be fitted successfully to the double-exponential curve, indicating the presence of two phases (compare the residual for single- and double-exponential fits). Other PL spin labels also showed the presence of two phases at that cholesterol mixing ratio. Results are consistent with the phase diagram shown in Fig. 1. Coexisting l_d and l_o phases are expected at the Chol/ESM mixing ratio of 1:4. Furthermore, the l_o-phase domain and CBD are expected to coexist at a mixing ratio of 3:1. However, the CBD cannot be discriminated using PL-analog spin labels, which do not partition into the pure cholesterol domain. In double-exponential fits in the presence of oxygen, shorter T_1 values for all PL-analog spin labels were assigned to the l_d phase, and longer values to the l_o phase. These assignments were confirmed by T_1 measurements. T_1 values measured at a Chol/ESM mixing ratio of 1:2 were nearly the same as longer T_1 values measured at a Chol/ESM mixing ratio of 1:4. T_1 values in the presence and absence of molecular oxygen were used to calculate values of the OTP (see Eq. S1) and to obtain profiles of the OTP across single or coexisting membrane phases and/or domains.

Discrimination of membrane phases and domains using cholesterol-analog spin labels

Because the CBD is a pure cholesterol domain (Fig. 1 *f*), it can only be discriminated with cholesterol-analog spin labels. For this purpose, we used CSL (in which the nitroxide moiety replaces the –OH group of cholesterol) and ASL (which is similar to CSL with the isooctyl chain replaced by the –OH group (see Fig. S1)). Both CSL and ASL should be anchored at the membrane surface by their –OH groups. However, ASL possesses two polar ends, and, in principle, both can be located in a polar headgroup region. The –OH group is more polar than the nitroxide moiety and is expected to be located in the headgroup region. However, the opposite orientation is possible, especially when the lipid composition of the membrane changes. This presents the question of whether the expected double-exponential SR signals of ASL in the presence of oxygen indicate 1), formation of coexisting domains (as shown in Fig. 1, *b* and *f*) or 2), the "upside-down" orientation of ASL. To clarify this problem, we measured local hydrophobicity around the nitroxide moiety of ASL in Chol/ESM membranes (with a mixing ratio between 0 and 3) and compared it to local hydrophobicity around the nitroxide moiety of CSL (Fig. 3). Hydrophobicity measured with

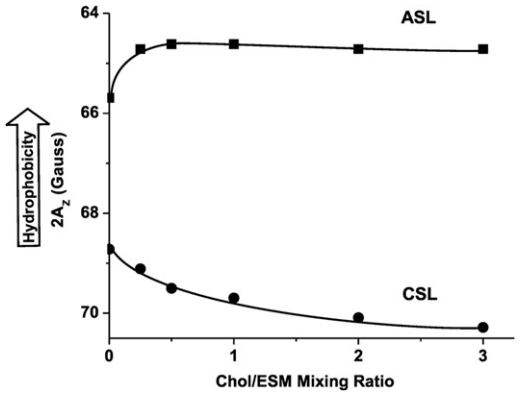

FIGURE 3 Hydrophobicity around the nitroxide moiety of ASL and CSL in membranes made of Chol/ESM membranes plotted as a function of Chol/ESM mixing ratio.

ASL does not change with an increase in cholesterol content (with the exception of a small increase after the addition of 25–30 mol % cholesterol). In contrast, hydrophobicity measured with CSL decreases with an increase in cholesterol content. Cholesterol molecules separate larger PL headgroups and increase water penetration to the polar headgroup region where the nitroxide moiety of CSL is located (14). In the CBD, the nitroxide moiety of CSL is fully exposed to the water phase (Fig. 1 *f*). The difference between $2A_Z$ values detected by ASL (~64.5 G) and CSL (~70.0 G) is so great that the orientation of ASL with the nitroxide moiety in the polar headgroup region (like CSL) should be detected at a high cholesterol content. The results allow us to infer that the nitroxide moiety of ASL is always located in the hydrophobic membrane center, independently of cholesterol content, and that ASL unambiguously detects two coexisting domains, not the distribution of ASL orientations (see (9) for more detail).

Fig. 4 shows representative SR signals of ASL (*A*) and CSL (*B*) in Chol/ESM membranes with a mixing ratio of 3:1 in the presence and absence of oxygen. SR signals were fitted using single and double exponentials and compared. The single-exponential fit was satisfactory for both ASL and CSL in deoxygenated membranes. For ASL in the presence of oxygen, the single-exponential fit was not satisfactory, whereas the double-exponential fit was excellent (compare the residual for single- and double-exponential fits). T_1 values from double-exponential curves were assigned to the l_o-phase domain (the shorter time constant) and to the CBD (the longer time constant) (see (7–9) for more detail). However, all SR signals obtained with CSL for membranes in the presence of oxygen were single exponentials (Fig. 4 *B*). Because CSL should be distributed between the l_o-phase domain and the CBD similar to cholesterol, we conclude that the collision rate between oxygen and the nitroxide moiety of CSL is the same in both domains (see also the discussion in (7).). Thus, the existence of the CBD in ESM membranes can be confirmed using ASL and oxygen, but not CSL.

To clarify this problem, we used NiEDDA, which strongly affects the T_1 values of spin labels with the nitroxide moiety at the membrane-water interface (like CSL). Fig. 4 *C* shows representative SR signals for CSL in the presence and absence of NiEDDA. In the presence of NiEDDA, a single-exponential fit was not satisfactory, whereas the double-exponential fit was excellent (compare the residual for single- and double-exponential fits). T_1s were assigned to the l_o-phase domain (the longer time constant) and to the CBD (the shorter time constant). Thus, the existence of the CBD can also be confirmed with CSL and NiEDDA as a relaxation agent. All SR signals obtained with ASL for membranes in the presence of NiEDDA were single exponentials, with the time constant nearly the same as in the absence of NiEDDA (data not shown). We conclude that NiEDDA does not penetrate to the depth at which the nitroxide moiety of ASL is located both in the l_o-phase domain and the CBD. These results are in agreement with hydrophobicity measurements for ASL presented in Fig. 3.

Final results for discriminating membrane domains with ASL and CSL are presented in Fig. 5. As expected, we detected two domains when the Chol/ESM mixing ratio was greater than the CST in the ESM bilayer. This display also confirmed our assignments of SR results to the l_o-phase domain and the CBD. Results presented in Fig. 5 *A* indicate that the OTP in the center of the CBD is about three to six times smaller than that in the center of the l_o-phase domain. Although CSL data show a single value for the OTP for all cholesterol contents, this does not mean that CSL detects a single homogeneous domain. Data indicate that the collision rate between the nitroxide moiety of CSL and oxygen

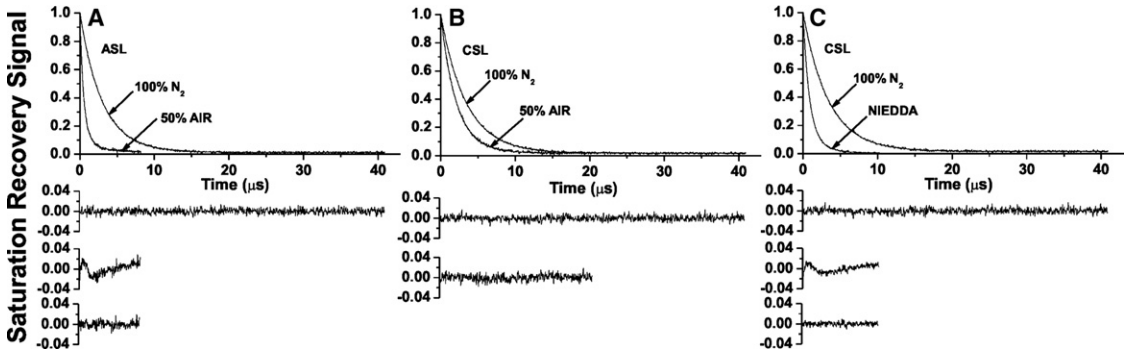

FIGURE 4 Representative SR signals with fitted curves and residuals for (*A*) ASL and (*B* and *C*) CSL in an ESM membrane with a Chol/ESM mixing ratio of 3. Signals were recorded for samples equilibrated with (*A–C*) 100% nitrogen, (*A–B*) with a gas mixture of 50% air and 50% nitrogen, and (*C*) in the presence of NiEDDA. For deoxygenated samples, SR signals were satisfactorily fit to a single-exponential function with time constants of (*A*) 3.00 ± 0.01 μs, (*B*) 3.41 ± 0.01 μs, and (*C*) 3.41 ± 0.01 μs (upper residuals are for single-exponential fit). The SR signal in the presence of molecular oxygen can be fitted satisfactorily with a single exponential function only for CSL with a time constant of (*B*) 2.12 ± 0.01 μs (lower residual is for single-exponential fit) and with double exponential curves for ASL with time constants of (*A*) 1.72 ± 0.07 μs and 0.48 ± 0.01 μs (the middle residual is for single- and the lower residual for double-exponential fits). The SR signal for CSL in the presence of NiEDDA can be fitted satisfactorily only with double-exponential curves with time constants of (*C*) 1.57 ± 0.04 μs and 0.74 ± 0.01 μs (the middle residual is for single- and the lower residual for double-exponential fits).

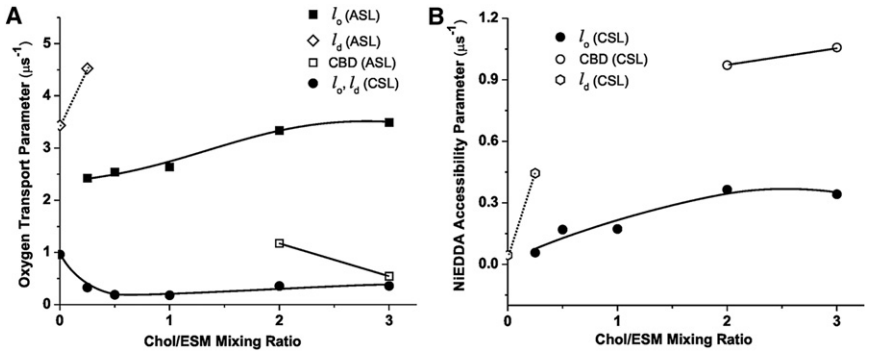

FIGURE 5 (*A*) The OTP for ASL and CSL and (*B*) the NiEDDA accessibility parameter for CSL in Chol/ESM membranes plotted as a function of the Chol/ESM mixing ratio.

in the l_o-phase domain and the CBD is the same. Thus, the value of the OTP obtained with CSL can be used for both domains to create profiles of the OTP. This hypothesis was confirmed by measurements with NiEDDA that show CSL is located in the l_o-phase domain and the CBD, and can discriminate these domains (Fig. 5 *B*). The nitroxide moiety of CSL is more exposed to collisions with NiEDDA when CSL is located in the CBD and the moiety is not protected by the umbrella effect of phospholipid headgroups (as in the l_o-phase domain). These results are in agreement with the hydrophobicity measurements presented in Fig. 3, which show that the polarity around the nitroxide moiety of CSL increases when the cholesterol content increases beyond the CST.

Interestingly, the dual-probe method using ASL and oxygen has also allowed us to discriminate coexisting l_d and l_o phases. Double-exponential signals were measured, and two values of the OTP were calculated for the Chol/ESM mixing ratio of 1:4 (Fig. 5 *A*). Furthermore, the use of CSL with NiEDDA has allowed us to discriminate coexisting l_d and l_o phases. Two values of the NiEDDA accessibility parameter at the Chol/ESM mixing ratio of 1:4 were given (Fig. 5 *B*).

Profile of the OTP across the l_d phase at different cholesterol contents

OTP profiles across the l_d phase were obtained in two distinct regions in the phase diagram (Fig. 1) 1), the l_d phase in the absence of cholesterol (Fig. 6 *a*); and 2), the l_d phase saturated with cholesterol that coexists with the l_o phase (~7.5 mol% cholesterol in the l_d phase for a Chol/ESM mixing ratio of 1:4 at 40°C; Fig. 6 *b*). OTP values obtained with ASL and CSL are also included in the profiles.

The profile for the l_d phase without cholesterol is a broad bell shape, with all values of the OTP greater than the OTP in water. OTP values in the membrane center are about two times larger than those close to the membrane surface. Comparison of this profile (Fig. 6 *a*) with that in the l_d phase containing ~7.5 mol % cholesterol (*upper profile* in Fig. 6 *b*) reveals that the OTP is much greater in the l_d phase containing the very small (~7.5 mol %) concentration of cholesterol. This is surprising not only because it is contrary to the general view that cholesterol increases alkyl chain order and suppresses molecular motion, but also because such a small concentration of cholesterol induced such large increases in the OTP. However, a similar increase in the OTP was induced by ~5 mol % cholesterol in the l_d phase of the DMPC membrane (3). Furthermore, we have previously shown that small amounts of cholesterol (< 5 mol %) increase alkyl-chain mobility (*gauche-trans* isomerization) in the l_d phase (see Fig. 3 in (49)). In that study, a strong rigidifying effect was observed for cholesterol in concentrations above 5 mol %. This enhanced mobility of the phospholipid spin label and OTP in the presence of very small amounts of cholesterol may be due to an impurity effect of cholesterol: it destroys cooperative, dynamic characteristics by forming the membrane of a single molecular species, which is particularly apparent in the middle of the bilayer where cholesterol induces vacant space.

Profile of the OTP across the l_o phase at different cholesterol contents

Detailed OTP profiles in the l_o phase were obtained with PL-analog spin labels in the five distinct regions indicated in the phase diagram of Fig. 1: 1), the l_o phase that coexists with the l_d phase (~30 mol % cholesterol in the domain for a Chol/ESM mixing ratio of 1:4; Fig. 6 *b*); 2), the l_o phase that constitutes the whole membrane and contains the lowest cholesterol concentration of 33 mol % (Fig. 6 *c*); 3), the l_o phase that constitutes the whole membrane with 50 mol % cholesterol (Fig. 6 *d*); 4), the l_o phase that is saturated with cholesterol (at 66 mol % cholesterol; Fig. 6 *e*); and 5), the l_o-phase domain that coexists with the CBD (~66 mol % cholesterol in the domain for a Chol/ESM mixing ratio of 3:1; Fig. 6 *f*). OTP values obtained with ASL and CSL are also included in the profiles.

Profiles for the l_o phase containing the lowest cholesterol concentration (Fig. 6, *b* and *c*) are not much different than those for the pure ESM membrane (Fig. 6 *a*). All profiles have a bell shape, with a gradual increase in the OTP toward the membrane center. The major difference is that in the l_o phase the OTP is 50–20% lower and closer to the membrane surface (T-, 5-, 7-, 9-PC positions). At deeper positions, the

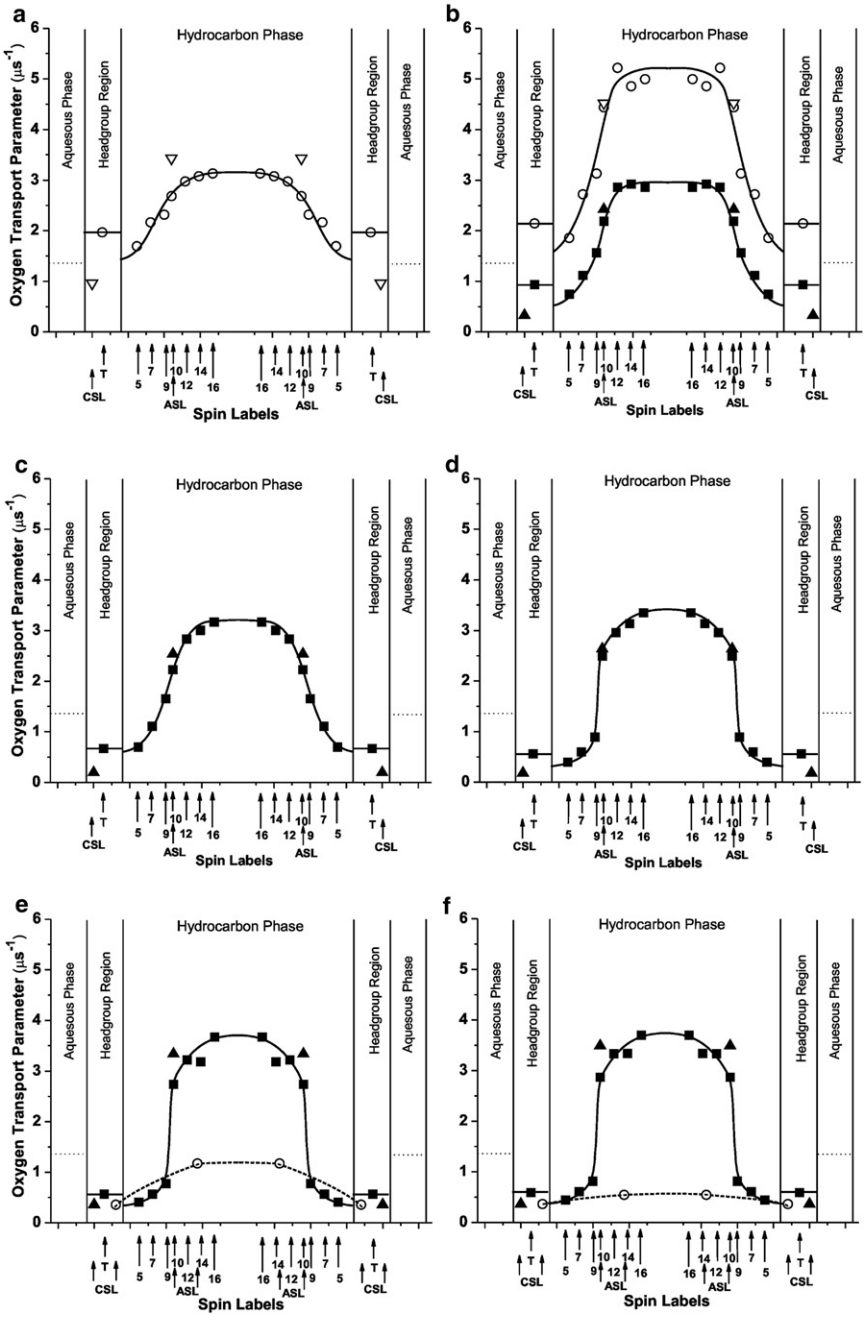

FIGURE 6 Profiles of the OTP for Chol/ESM membranes obtained at Chol/ESM mixing ratios of (*a*) 0, (*b*) 1:4, (*c*) 1:2, (*d*) 1:1, (*e*) 2:1, and (*f*) 3:1 (schemes for membrane structures are shown in Fig. 1). Dotted lines indicate the OTP in the aqueous phase.

OTP values are very similar. Further increase in the overall cholesterol content—up to the CST—induced a dramatic change in the OTP profile (Fig. 6, *d* and *e*), decreasing the OTP close to the membrane surface and increasing it in the membrane center. As a result, the OTP profile became almost rectangular, with a sharp 3–4-fold change in its value between the C9 and C10 positions. For membranes saturated with cholesterol, overall change in the OTP across the membrane was as large as a factor of ~9. OTP values from depths close to the membrane surface were as low as those observed in gel-phase membranes, and values from the membrane center were as high (or even higher) as those observed for the pure ESM membrane. The abrupt increase in the OTP occurs at the depth at which the rigid tetracyclic cholesterol structure is immersed. Increase in cholesterol content beyond the CST does not cause any further change in the OTP profile in the l_o-phase domain (Fig. 6 *f*), indicating that properties of the l_o-phase domain are minimally affected by the CBD.

Profile of the OTP across the CBD

Because only ASL and CSL can be located in the CBD, an approximate profile of the OTP can be drawn based on OTP

values obtained with these spin labels. Two OTP values were obtained with ASL. One fits perfectly into the profile across the coexisting l_o-phase domain, and the other indicates the OTP in the CBD. As was explained earlier, OTP values obtained with CSL are the same in the l_o-phase domain and the CBD. Profiles of the OTP across the CBD are included in Fig. 6, *e* and *f*. Profiles in Fig. 6 *f* were obtained at a Chol/ESM mixing ratio of 3:1, at which the CBD coexists with the l_o-phase domain. (The CBD is the pure cholesterol bilayer, and the surrounding l_o-phase domain is the ESM bilayer saturated with cholesterol (66 mol %)). Under these conditions, 66% of cholesterol molecules should saturate the ESM bilayer, and 33% should form the CBD. Values of the OTP in the center of the CBD are about three times lower than in the water phase and seven times lower than in the center of the l_o-phase domain. These OTP values are similar to values previously obtained by us for the CBD formed in lens lipid membranes (7,8) and in binary mixtures of cholesterol with PLs (9). Our conclusion that the CBD can form a barrier to oxygen transport is supported.

The CBD was also unexpectedly detected at a Chol/ESM mixing ratio of 2:1, which reaches the CST in ESM membranes. The OTP profile across the CBD is presented in Fig. 6 *e* based on these measurements. It differs significantly from that in Fig. 6 *f*, showing OTP values more than two times greater in the CBD center. Profiles in Fig. 6 *e* were drawn based on measurements for cholesterol contents close to the CST. Thus, only a small amount of cholesterol is involved in the formation of the CBD. With this condition, the CBD is small. The high exchange rate of lipid molecules between the small CBD and surrounding l_o-phase domain and/or high frequency of formation and dissipation of the CBD should make the properties of the CBD more closely resemble those of the l_o-phase domain. This is in agreement with our earlier statement that CBDs are highly dynamic domains (9).

GENERAL DISCUSSION

After reviewing the literature (20–22,50) and weighting our results, it was concluded that rafts can be considered domains of a l_o phase. On the basis of this concept, we believe that efforts to characterize l_o phases and domains extensively are important. Because the membrane (and, thus, the l_o phase and domain) is not really a two-dimensional structure, knowledge of the molecular dynamics and structures in the direction of the depth in the membrane is especially important.

We previously investigated properties of ESM membranes as a function of cholesterol content from 0 to 50 mol % using only one spin label (4). The nitroxide moiety was located at the C5 position where we expected the strongest effects of cholesterol. We distinguished the l_o phase from the l_d phase (and the s_o phase) and obtained values of the OTP for these phases at the C5 position. We were also able to confirm in Chol/ESM membranes positions of the boundaries between regions with coexisting l_d and l_o phases or s_o and l_o phases and the region with a single l_o phase. In our present research, which completes the studies presented in our previous work (4), we obtained detailed profiles of the OTP across single or coexisting phases in ESM membranes for different Chol/ESM mixing ratios from 0 to 3. At cholesterol contents lower than 33 mol % (Fig. 1 *b*), we were able to discriminate l_o and l_d phases using both PL- and cholesterol-analog spin labels. However, at cholesterol contents equal to or >33 mol % (Fig. 1, *c–e*), both types of spin labels indicated a homogenous phase. Our data are in agreement with data obtained for Chol/ESM and Chol/PSM membranes using solid-state ^{2}H NMR spectroscopy (43). When the cholesterol content was equal to or exceeded the CST in the ESM membrane (Fig. 1, *e* and *f*), we were also able to discriminate and characterize the CBD (see, however, the explanation in the section, Profile of the OTP across the CBD). This allowed us to make the hypothetical extension of the phase diagrams for Chol/ESM presented earlier (4,39,51) to the area of the membrane overloaded with cholesterol, where cholesterol not only saturates the PL bilayer but also forms the immiscible CBD.

Our data confirmed that the properties of different membrane phases and domains are strongly affected by cholesterol concentration, and that this effect is different at different depths in the lipid bilayer. The most pronounced changes were observed for the l_o phase in which the OTP profile changed from a bell shape to a rectangular shape. The fluidity of the l_o phase saturated with cholesterol from the membrane surface to the depth of C9 is suppressed to the level of fluidity in the gel-phase membrane, whereas in the membrane center, fluidity is comparable to that in the center of the fluid-phase membrane without cholesterol. It should be noted that the fluidity measured here is determined by translational motion of the oxygen molecule within the membrane. This work complements our previous work (3) in which we characterize the binary mixture of DMPC and cholesterol. Data obtained in these works should be used as a reference point to compare the properties of lipid phases and domains in model and biological membranes.

Cholesterol-mediated lipid interactions have important effects on the lateral organization of PLs in the membrane. They increase the molecular order of PL alkyl chains, increase membrane thickness, and modulate the packing of lipids in the membrane. This so-called "condensation effect" is much stronger for saturated PLs than for unsaturated PLs. These differences are clearly seen in profiles of the OTP. OTP values measured from the membrane surface to the depth of C9 for 1-palmitoyl-2-oleoyl-*sn*-glycero-3-phosphocholine (POPC) (6), DMPC (3), and ESM membranes saturated with cholesterol (the work presented here) show that the most tightly packed lipids are in the ESM membrane. Values of the OTP obtained at 40°C for 5-PC in Chol/POPC, Chol/DMPC, and Chol/ESM membranes are ~0.9, ~0.65, and ~0.4 μs^{-1}, respectively. However, in the membrane center,

saturating amounts of cholesterol do not change the OTP (as in POPC and DMPC membranes) or even increase it (as in ESM membranes). There is an apparent discrepancy between our observations and the work of Bunge et al. (24) who showed, using cholesterol analog spin labels with the nitroxide moiety attached to the end of the isooctyl chain, which in the membrane center cholesterol also induces a greater order in PSM than in POPC. The order parameter (the static membrane parameter) cannot differentiate the effects of cholesterol at different depths, whereas the dynamic parameter (namely, the OTP) clearly shows the differences between the membrane region where the cholesterol ring structure is located and the deeper region where the isooctyl chain of cholesterol is located (see (3,46) for more discussion).

These data also contribute to our research on lens lipid membranes. PL compositions of these membranes change significantly between species, with age, and with location in the lens (cortex versus nucleus). For example, the total PL extract from the lenses of animals with a short life span (i.e., a mouse or rat) contains ~45% PC and only ~15% SM. From human lenses, the total PL extract contains ~11% PC and 66% SM (32). The ratio of PC/SM in two-year-old cow lens cortex and nucleus is 0.66–2.0 and 0.21–0.5, respectively (8). The cholesterol content in all lens lipid membranes is close to the CST or higher (8,30). We previously obtained detailed profiles of membrane properties across POPC membranes with cholesterol contents close to or exceeding the CST, which occurs at a Chol/POPC mixing ratio of 1 (6). Here, we obtained detailed profiles of the OTP across ESM membranes at a cholesterol mixing ratio from 0 to 3. This allowed us to investigate ESM membranes in conditions similar to those in lens lipid membranes, keeping in mind that the CST in ESM membranes is at a Chol/ESM mixing ratio of 2 (34). We were able to discriminate the CBD at a Chol/ESM mixing ratio of 3, even as well at a mixing ratio of 2. In the latter case, CBDs were small and/or lipid exchange between them and a surrounding membrane was fast. In the former case, the properties of CBDs were similar to those reported earlier (9). OTP profiles across the surrounding ESM bilayer saturated with cholesterol were rectangular in shape, with an abrupt increase in OTP value between C9 and C10, and did not change when the cholesterol mixing ratio was increased from 2 to 3 and the CBD was formed. Profiles were practically identical to those obtained for lens lipid membranes (6–8) and across POPC membranes saturated with cholesterol or obtained in the presence of the CBD (6).

SUPPORTING MATERIAL

One figure and additional text are available at http://www.biophysj.org/biophysj/supplemental/S0006-3495(11)00844-7.

This work was supported by grants EY015526, TW008052, EB002052, and EB001980 of the National Institutes of Health.

REFERENCES

1. Subczynski, W. K., and A. Kusumi. 2003. Dynamics of raft molecules in the cell and artificial membranes: approaches by pulse EPR spin labeling and single molecule optical microscopy. *Biochim. Biophys. Acta.* 1610:231–243.
2. Kawasaki, K., J.-J. Yin, …, A. Kusumi. 2001. Pulse EPR detection of lipid exchange between protein-rich raft and bulk domains in the membrane: methodology development and its application to studies of influenza viral membrane. *Biophys. J.* 80:738–748.
3. Subczynski, W. K., A. Wisniewska, …, A. Kusumi. 2007. Three-dimensional dynamic structure of the liquid-ordered domain in lipid membranes as examined by pulse-EPR oxygen probing. *Biophys. J.* 92:1573–1584.
4. Wisniewska, A., and W. K. Subczynski. 2008. The liquid-ordered phase in sphingomyelin-cholesterol membranes as detected by the discrimination by oxygen transport (DOT) method. *Cell. Mol. Biol. Lett.* 13:430–451.
5. Kusumi, A., W. K. Subczynski, …, H. Merkle. 1986. Spin-label studies on phosphatidylcholine-cholesterol membranes: effects of alkyl chain length and unsaturation in the fluid phase. *Biochim. Biophys. Acta.* 854:307–317.
6. Widomska, J., M. Raguz, …, W. K. Subczynski. 2007. Physical properties of the lipid bilayer membrane made of calf lens lipids: EPR spin labeling studies. *Biochim. Biophys. Acta.* 1768:1454–1465.
7. Raguz, M., J. Widomska, …, W. K. Subczynski. 2008. Characterization of lipid domains in reconstituted porcine lens membranes using EPR spin-labeling approaches. *Biochim. Biophys. Acta.* 1778:1079–1090.
8. Raguz, M., J. Widomska, …, W. K. Subczynski. 2009. Physical properties of the lipid bilayer membrane made of cortical and nuclear bovine lens lipids: EPR spin-labeling studies. *Biochim. Biophys. Acta.* 1788:2380–2388.
9. Raguz, M., L. Mainali, …, W. K. Subczynski. 2011. The immiscible cholesterol bilayer domain exists as an integral part of phospholipid bilayer membranes. *Biochim. Biophys. Acta.* 1808:1072–1080.
10. Widomska, J., M. Raguz, and W. K. Subczynski. 2007. Oxygen permeability of the lipid bilayer membrane made of calf lens lipids. *Biochim. Biophys. Acta.* 1768:2635–2645.
11. Subczynski, W. K., J. Widomska, …, A. Kusumi. 2007. Saturation-recovery electron paramagnetic resonance discrimination by oxygen transport (DOT) method for characterizing membrane domains. *In* Methods in Molecular Biology, Lipid Rafts.. Humana Press, Totowa, NJ. 143–157.
12. Subczynski, W. K., M. Raguz, and J. Widomska. 2010. Studying lipid organization in biological membranes using liposomes and EPR spin labeling. *Methods Mol. Biol.* 606:247–269.
13. Subczynski, W. K., R. N. Lewis, …, A. Kusumi. 1998. Molecular organization and dynamics of 1-palmitoyl-2-oleoylphosphatidylcholine bilayers containing a transmembrane alpha-helical peptide. *Biochemistry.* 37:3156–3164.
14. Subczynski, W. K., A. Wisniewska, …, A. Kusumi. 1994. Hydrophobic barriers of lipid bilayer membranes formed by reduction of water penetration by alkyl chain unsaturation and cholesterol. *Biochemistry.* 33:7670–7681.
15. Kusumi, A., W. K. Subczynski, and J. S. Hyde. 1982. Oxygen transport parameter in membranes as deduced by saturation recovery measurements of spin-lattice relaxation times of spin labels. *Proc. Natl. Acad. Sci. USA.* 79:1854–1858.
16. Subczynski, W. K., J. S. Hyde, and A. Kusumi. 1989. Oxygen permeability of phosphatidylcholine-cholesterol membranes. *Proc. Natl. Acad. Sci. USA.* 86:4474–4478.
17. Ashikawa, I., J.-J. Yin, …, A. Kusumi. 1994. Molecular organization and dynamics in bacteriorhodopsin-rich reconstituted membranes: discrimination of lipid environments by the oxygen transport parameter using a pulse ESR spin-labeling technique. *Biochemistry.* 33:4947–4952.

18. Ridgway, N. D. 2000. Interactions between metabolism and intracellular distribution of cholesterol and sphingomyelin. *Biochim. Biophys. Acta.* 1484:129–141.

19. Pike, L. J. 2006. Rafts defined: a report on the Keystone Symposium on Lipid Rafts and Cell Function. *J. Lipid Res.* 47:1597–1598.

20. Edidin, M. 2003. The state of lipid rafts: from model membranes to cells. *Annu. Rev. Biophys. Biomol. Struct.* 32:257–283.

21. London, E. 2002. Insights into lipid raft structure and formation from experiments in model membranes. *Curr. Opin. Struct. Biol.* 12: 480–486.

22. Simons, K., and W. L. Vaz. 2004. Model systems, lipid rafts, and cell membranes. *Annu. Rev. Biophys. Biomol. Struct.* 33:269–295.

23. Frazier, M. L., J. R. Wright, …, P. F. Almeida. 2007. Investigation of domain formation in sphingomyelin/cholesterol/POPC mixtures by fluorescence resonance energy transfer and Monte Carlo simulations. *Biophys. J.* 92:2422–2433.

24. Bunge, A., P. Müller, …, D. Huster. 2008. Characterization of the ternary mixture of sphingomyelin, POPC, and cholesterol: support for an inhomogeneous lipid distribution at high temperatures. *Biophys. J.* 94:2680–2690.

25. Heberle, F. A., J. Wu, …, G. W. Feigenson. 2010. Comparison of three ternary lipid bilayer mixtures: FRET and ESR reveal nanodomains. *Biophys. J.* 99:3309–3318.

26. Almeida, P. F. F. 2009. Thermodynamics of lipid interactions in complex bilayers. *Biochim. Biophys. Acta.* 1788:72–85.

27. Veatch, S. L., and S. L. Keller. 2003. Separation of liquid phases in giant vesicles of ternary mixtures of phospholipids and cholesterol. *Biophys. J.* 85:3074–3083.

28. McConnell, H. M., and A. Radhakrishnan. 2003. Condensed complexes of cholesterol and phospholipids. *Biochim. Biophys. Acta.* 1610:159–173.

29. Polozov, I. V., and K. Gawrisch. 2006. Characterization of the liquid-ordered state by proton MAS NMR. *Biophys. J.* 90:2051–2061.

30. Li, L. K., L. So, and A. Spector. 1987. Age-dependent changes in the distribution and concentration of human lens cholesterol and phospholipids. *Biochim. Biophys. Acta.* 917:112–120.

31. Borchman, D., and M. C. Yappert. 2010. Lipids and the ocular lens. *J. Lipid Res.* 51:2473–2488.

32. Deeley, J. M., T. W. Mitchell, …, R. J. Truscott. 2008. Human lens lipids differ markedly from those of commonly used experimental animals. *Biochim. Biophys. Acta.* 1781:288–298.

33. Epand, R. M. 2003. Cholesterol in bilayers of sphingomyelin or dihydrosphingomyelin at concentrations found in ocular lens membranes. *Biophys. J.* 84:3102–3110.

34. Epand, R. M., A. D. Bain, …, E. Wachtel. 2002. Properties of mixtures of cholesterol with phosphatidylcholine or with phosphatidylserine studied by (13)C magic angle spinning nuclear magnetic resonance. *Biophys. J.* 83:2053–2063.

35. Huang, J., J. T. Buboltz, and G. W. Feigenson. 1999. Maximum solubility of cholesterol in phosphatidylcholine and phosphatidylethanolamine bilayers. *Biochim. Biophys. Acta.* 1417:89–100.

36. Bach, D., and E. Wachtel. 2003. Phospholipid/cholesterol model membranes: formation of cholesterol crystallites. *Biochim. Biophys. Acta.* 1610:187–197.

37. Müller-Landau, F., and D. A. Cadenhead. 1979. Molecular packing in steroid-lecithin monolayers, part I: Pure films of cholesterol, 3-doxylcholestane, 3-doxyl-17-hydroxyl-androstane, tetradecanoic acid and dipalmitoyl-phosphatidylcholine. *Chem. Phys. Lipids.* 25:299–314.

38. Almeida, P. F. F., W. L. C. Vaz, and T. E. Thompson. 1992. Lateral diffusion in the liquid phases of dimyristoylphosphatidylcholine/cholesterol lipid bilayers: a free volume analysis. *Biochemistry.* 31: 6739–6747.

39. de Almeida, R. F., A. Fedorov, and M. Prieto. 2003. Sphingomyelin/phosphatidylcholine/cholesterol phase diagram: boundaries and composition of lipid rafts. *Biophys. J.* 85:2406–2416.

40. Kusumi, A., W. K. Subczynski, and J. S. Hyde. 1982. Effects of pH on ESR spectra of stearic acid spin labels in membranes: probing the membrane surface. *Fed. Proc.* 41:1394.

41. Papahadjopoulos, D. 1968. Surface properties of acidic phospholipids: interaction of monolayers and hydrated liquid crystals with uni- and bivalent metal ions. *Biochim. Biophys. Acta.* 163:240–254.

42. Buboltz, J. T. 2009. A more efficient device for preparing model-membrane liposomes by the rapid solvent exchange method. *Rev. Sci. Instrum.* 80:124301–124305.

43. Bartels, T., R. S. Lankalapalli, …, M. F. Brown. 2008. Raftlike mixtures of sphingomyelin and cholesterol investigated by solid-state 2H NMR spectroscopy. *J. Am. Chem. Soc.* 130:14521–14532.

44. Benatti, C. R., M. T. Lamy, and R. M. Epand. 2008. Cationic amphiphiles and the solubilization of cholesterol crystallites in membrane bilayers. *Biochim. Biophys. Acta.* 1778:844–853.

45. Hyde, J. S., and W. K. Subczynski. 1989. Spin-label oximetry. *In* Biological Magnetic Resonance. L. J. Berliner and J. Reuben, editors. Plenum Press, New York. 399–425.

46. Yin, J. J., and W. K. Subczynski. 1996. Effects of lutein and cholesterol on alkyl chain bending in lipid bilayers: a pulse electron spin resonance spin labeling study. *Biophys. J.* 71:832–839.

47. Subczynski, W. K., C. C. Felix, …, J. S. Hyde. 2005. Concentration by centrifugation for gas exchange EPR oximetry measurements with loop-gap resonators. *J. Magn. Reson.* 176:244–248.

48. Quinn, P. J., and C. Wolf. 2009. Hydrocarbon chains dominate coupling and phase coexistence in bilayers of natural phosphatidylcholines and sphingomyelins. *Biochim. Biophys. Acta.* 1788:1126–1137.

49. Subczynski, W. K., and A. Kusumi. 1986. Effects of very small amounts of cholesterol on gel-phase phosphatidylcholine membranes. *Biochim. Biophys. Acta.* 854:318–320.

50. Ge, M., K. A. Field, …, J. H. Freed. 1999. Electron spin resonance characterization of liquid ordered phase of detergent-resistant membranes from RBL-2H3 cells. *Biophys. J.* 77:925–933.

51. Collado, M. I., F. M. Goñi, …, D. Marsh. 2005. Domain formation in sphingomyelin/cholesterol mixed membranes studied by spin-label electron spin resonance spectroscopy. *Biochemistry.* 44:4911–4918.